Electron-Beam Detection of Bits Reversibly Recorded on Epitaxial InSe/GaSe/Si Phase-Change Diodes

Alison Chaiken[*1], Gary A. Gibson, John Chen[*2], Bao S. Yeh[*2], J.B. Jasinski[*3], Z. Liliental-Weber[*3], K. Nauka, C.C. Yang, D.D. Lindig[*4] and S. Subramanian[*4]

Hewlett-Packard Laboratories, 1501 Page Mill Rd., Palo Alto, CA 94304 U.S.A

(Received)

We demonstrate a data read-back scheme based on electron-beam induced current in a data storage device that utilizes thermal recording onto a phase-change medium. The phase-change medium is part of a heterojunction diode whose local charge-collection efficiency depends on the crystalline or amorphous state of a bit. Current gains up to 65 at 2 keV electron beam energy have been demonstrated using InSe/GaSe/Si epitaxial diodes. Fifteen write-erase cycles are obtained without loss of signal contrast by using a protective cap layer and short write pulses. 100 write-erase cycles have been achieved with some loss of contrast. Erasure times for the bits are longer than in similar polycrystalline In-Se media films. Possible reasons for the long erasure times are discussed in terms of a nucleation- or growth-dominated recrystallization. Prospects for extension to smaller bit sizes using electron-beam writing are considered.

KEYWORDS: data storage, phase change, electron beam, InSe, GaSe, recrystallization, nucleation, optical recording, scanned probe

[*1] E-mail address: chaiken@hpl.hp.com

[*2] Present address: Imaging and Printing Group, Hewlett-Packard, Corvallis OR U.S.A.

[*3] Present address: Materials Sciences Division, Lawrence Berkeley National Laboratory, Berkeley, CA U.S.A.

[*4] Present address: Imaging and Printing Group, Hewlett-Packard, Boise ID U.S.A.

1. Introduction

Data storage products have bit cells whose dimensions are rapidly approaching the length scales that are typically associated with nanotechnology. Disk drives record information via magnetic domains with lengths in the range of 27 to 38 nm and track pitches in the range of 115 to 280 nm.[1)] A recent typical digital versatile disc (DVD) prototype system with a 405 nm light source employed an amorphous bit length of 126.9 nm with a land/groove width of 340 nm.[2)] Advanced recording schemes that propose to drive bit sizes even smaller have incorporated the near-field scanning optical microscope,[3)] nanofocusing probes[4)] and solid-immersion lens[5)] technologies. Several other groups have proposed using microfabricated arrays of scanned probes to record onto phase-change materials similar to those used as commercial optical recording media. For example, crystalline bits in an amorphous GeSbTe film have been created using near-field optics,[6)] current pulses from a conducting tip,[7)] and thermal pulses from heated tips.[8)] Formation of 250-nm-diameter amorphous bits in a crystalline GeSbTe medium was demonstrated using a novel very-small-aperture laser.[9)] None of these phase-change-based efforts include a demonstration of bit erasure. A myriad of scanned-probe recording schemes based on other kinds of media have also been proposed.[10,11)]

Another possible method of obtaining ultrahigh data densities is to record with focused electron beams rather than with optical sources.[12–14)] In combination with a scanned micro-electro-mechanical platform for the media, the use of electron emitters for writing and reading makes high data rates and storage densities possible.[14)] As envisioned, electron-beam writing on phase-change media is fundamentally similar to optical recording in that the state of the material (crystalline or amorphous) is used to store information. The material state is cycled reversibly through use of an appropriately tailored heat pulse.[15)] However, an electron beam readout cannot detect phase-changed bits via contrast in reflectivity as is done in conventional optical recording. We have developed an electron-beam based read-back method in which the phase-change material is incorporated into a rectifying diode whose current is monitored by an external circuit. A major advantage of this approach is that it provides an intrinsic gain mechanism within the

storage medium. This gain results from the fact that the number of electron-hole pairs created by an electron beam of energy E_b incident on a semiconductor of energy gap E_g is approximately $E_b/(2.1E_g + 1.3)$.[16,17] Accordingly, signal currents much larger than the incident beam current can be realized even for moderate carrier collection efficiencies in the storage medium diode and for the sub-keV beam energies that can be produced in a practical integrated-circuit electron emitter.

A storage medium for electron-beam recording must provide the writability, erasibility and archivability of traditional optical phase-change media. These constraints imply that the storage layer must have a moderate melting temperature and a high glass transition temperature, and must recrystallize rapidly at high temperatures and slowly at ambient temperatures.[18] In addition, the medium device must permit electron-beam discrimination between the crystalline and amorphous states at small length scales. Our design for the medium uses a heterojunction diode whose top layer is a well-studied optical recording material. The regions of the diode where this phase-change layer is crystalline have a high collection efficiency for minority carriers generated by the incident read-beam electrons. The regions of the diode with an amorphous surface have a low collection efficiency due to the reduced carrier mobilities and lifetimes in the amorphous state. The challenge then is to fabricate a diode that has appreciable collection efficiency in the crystalline state and where the top layer is one of the IV-VI,[18] III-VI[19] or V-VI[20] semiconductors that have usable phase-change properties. Initial efforts focused on the use of GeSbTe/Si diodes because GeTe-Sb_2Te_3 pseudobinaries (GST) are the most widely employed phase-change media.[21] However, GST is a highly defective, small-gap semiconductor and diodes formed from this material have high leakage currents and unacceptably low collection efficiencies.[22]

Noise due to medium inhomogeneity is a major concern in any ultrahigh density recording device. In magnetic recording noise has been minimized by utilizing media with ever smaller grain sizes.[23] Shrinking the size of grains will not work with a medium that is an electronic device as a granular semiconductor will likely have poor charge-collection efficiency. The obvious alternative is to select an epitaxial medium film with as few defects as possible. Among the identified phase-change materials, only InSe has been

grown epitaxially on silicon.[24] Previous authors have phase-cycled the optical reflectivity of polycrystalline InSe films up to 10^6 times.[19] Sánchez-Royo and coworkers have measured the photoresponse of rectifying diodes consisting of InSe films grown on GaSe single crystals.[25] In addition, GaSe has been grown epitaxially on Si(111),[26] suggesting the possibility of a high-quality InSe/GaSe heterojunction diode device on Si. InSe and GaSe are layered semiconductors with anisotropic thermal and electronic properties.[27]

The quasi-2D structure of InSe and GaSe results in a reduced density of the surface and interface dangling bonds that can cause charge carrier recombination[27] and impede the collection of carriers generated near the surface by a low-energy electron read beam. These properties make InSe a favorable if atypical choice for a phase-change medium. In this paper we report on an optical recording study of epitaxial InSe/GaSe/Si(111) heterojunction diodes and the successful demonstration of electronic detection of amorphous bits over multiple write-erase cycles. Optical marking has been used as a surrogate for electron-beam marking while higher-power, focused electron-beam sources are under development.[12]

2. Experimental Methods

Guided by previous reports of the epitaxial growth of InSe on GaSe[28,29] and of GaSe on Si(111),[26] the InSe/GaSe film stack was grown by molecular beam epitaxy on p-Si(111) wafers from elemental Knudsen-cell sources. The Si wafers were cleaned using a buffered-oxide etch or an ethanol/HF mixture. Typical growth temperatures were 500-550 °C for the GaSe and 450 °C for the InSe. Growth rates were on the order of 0.1 nm/s. Four-circle X-ray diffraction measurements confirm the expected epitaxial structure of the films, consisting of layered InSe and GaSe. Electron diffraction and high-resolution transmission electron microscopy (TEM) images reveal that these films consist primarily of the rhombohedral polytypes of InSe and GaSe, although some stacking faults are observed.[30] Energy-dispersive X-ray analysis (EDX) shows that small particles on the surfaces of some films are In-rich precipitates even though Rutherford backscattering (RBS) indicates an average stoichiometry close to 1:1. Similar In droplets have been observed in the growth of InSe on GaAs[31] and on GaSe single crystals.[25] The origin of the In inclusions is cur-

rently unknown and will be studied further in a growth optimization effort using a newly installed Se cracker source. The energy gap and excitonic behavior of some samples were studied using photoreflectance and photoluminescence. Photoreflectance showed a zero-crossing and photoluminescence showed a peak near 1.2-1.25 eV,[32] similar to previously published results.[33,34]

InSe film thicknesses were usually in the 50-100 nm range, while GaSe thicknesses were typically 5-10 nm.

Molybdenum and carbon top contacts were sputtered at a low power. Molybdenum is an ohmic, minimally reactive contact material for the chalcogenide semiconductor $CuInSe_2$.[35] Because of its low mass-density, carbon can be made reasonably transparent to low-energy electrons while still providing adequate electrical conductivity. Some contacts covered the entire top surface of the approximately 1 cm^2 specimens while other contacts were smaller, lithographically defined pads. The best compromise between eraseability and electron-beam contrast was obtained in regions where the Mo cap thickness was in the range of 2-3 nm as determined by RBS measurements. SiO_2 secondary capping layers were sometimes added via RF sputtering from a silica target. SiO_2 could not be used alone as a capping layer due to problems with charging. A combination of 3 nm Mo plus 3 nm SiO_2 was used except as noted. A tapered Mo cap of similar but variable thickness was used in a few experiments.

Laser marking was accomplished using one of two systems. One system uses the 488 nm line from an Ar ion laser with a final microscope objective of numerical aperture (NA) 0.8 whose position is controlled by a four-quadrant-detector focus-servo system. Photocurrent and reflectivity maps were acquired by scanning the focused beam over the device with a low (70 μW) power. The dark current has been subtracted from the photoresponse data. Laser pulse shape was controlled using an acoustic-optic modulator and was monitored using an avalanche photodiode. The minimum width for square pulses was measured to be 12 ns. Reflectivity was calibrated using Si, Ge and Al standards. Focused beam width was measured with an oscillating knife edge profiler and found to be 0.36±0.01 μm. The second laser marking system used a 400 nm laser diode with an NA = 0.65 final objective.

Electron-beam-induced-current (EBIC) measurements were performed in a scanning

electron microscope (SEM) using incident energies from 0.7-2 keV. The dimensionless EBIC gain was defined to be the difference between the irradiated current and the dark current normalized to the incident beam current. The incident beam current was monitored using a Faraday cup. Most experiments were performed with zero bias on the diode structure. In the EBIC maps, a darker gray always indicates a lower current collected in the external circuit. An electron backscatter diffraction (EBSD) camera from TSL was used to acquire and analyze Kikuchi patterns from the surface of some specimens. Cathodoluminescence measurements over the range from 0.73-1.55 eV were performed in the SEM using an Oxford Instruments spectrometer at a sample temperature of 85 K. All other reported measurements were taken at room temperature and all laser marking experiments were performed in air. Furnace annealing of selected specimens was performed in a flowing Ar 93%-H_2 7% atmosphere.

3. Results

3.1 Electronic properties of the epitaxial diodes

Fig. 1 shows current-voltage curves for a typical InSe/GaSe/Si heterojunction diode. Given that undoped InSe is n-type[36)] while undoped GaSe is p-type,[37)] the shape of the curve is as anticipated. The dark rectification ratio at 1 V bias is 190. The photoinduced current at 0.5 V reverse bias is 38 times the dark current and the open-circuit voltage V_{oc} is -0.4 V with only about 25 μW of 488 nm light penetrating the cap to reach the small illuminated area. Due to unoptimized contacts and doping, the high series resistance of the diode in forward bias limits the fill factor derived from Fig. 1 to only 0.16. On a comparable device (a heterojunction formed from a 120 nm thick epitaxial InSe film grown on a GaSe single crystal) under AM2 conditions, J.F. Sánchez-Royo *et al.* reported a V_{oc} of 0.22 V and a fill factor of 0.30.[25)] The significant photoresponse of the heterojunction in reverse bias indicates that this material combination is a promising candidate for use as an electron-beam recording medium.

3.2 Electronic detection of amorphous bits

Fig. 2 displays results from a study of the write-power threshold. Marks were written with square 30 ns laser pulses of varying power and then scanned with a focused 70 μW

laser beam while simultaneously monitoring reflectivity and photocurrent. The photocurrent of the laser-written marks decreases monotonically with pulse powers above 5.1 mW, while the reflectivity of the marks is above the background for powers of 6.4 mW or less, and below that of the background for powers of 6.8 mW or more. These data suggest a damage threshold of 6.6 mW and an amorphization threshold near 5.1 mW. Because the same wavelength is used for marking and imaging, there's a danger of overestimating the marking threshold due to spatial undersampling of the marks. However, EBIC measurements performed on a wide variety of films and passivation layers consistently indicate the same marking threshold as photocurrent measurements. Amorphization thresholds were consistently between 5 and 7 mW for 50-100 nm thick InSe films with 3-5 nm Mo cap layers. Marking and damage power thresholds depend strongly on the cap thickness due to the high absorption of blue light in the metal layer.

A cross-sectional transmission electron microscopy image of a larger diameter, longer pulse-duration laser mark is shown in Fig. 3. Smaller marks made with more characteristic amorphization-pulse parameters were difficult to find in TEM cross-sectional specimens. The contrast between the amorphous region and the surrounding crystalline matrix is clear in (a). The diffraction pattern shown in (b) confirms that the mark is in fact amorphous. The diffraction pattern of the nearby unperturbed matrix is shown for comparison in (c). The small particles that are embedded in the amorphous regions are likely crystallites that formed during TEM sample preparation. An attempt to image these particles at high magnification failed due to unintentional e-beam modification of the amorphous material (discussed further below). The crystallites do not grow during TEM examination (as shown in Fig. 10 below). No signs of delamination or cracking are apparent. EDX measurements performed in the TEM indicate some diffusion of In into the GaSe in this sample, but this interdiffusion is not increased beneath the laser marks.[30]

Changes in the surface profile associated with the amorphization were anticipated due to a previous study that showed a linear relationship between depth of amorphization and topographic changes detected by atomic force microscopy (AFM).[38] The authors found a 6% volumetric expansion upon amorphization of $Ge_2Sb_2Te_5$.[38] Surprisingly, corresponding AFM studies of large arrays of laser marks made on our InSe/GaSe/Si(111) samples

with 30 ns pulses and near-threshold powers showed less than a 1% change in topography.

Higher powers and longer pulsewidths consistently created holes.

Fig. 4 shows EBIC and secondary electron images of laser marks made with 9.6 mW, 30 ns amorphization pulses on a device with a 8 nm Mo plus 5 nm SiO_2 cap. In the EBIC image (Fig. 4(a)) the small marks are about 250 nm in diameter and show high contrast. Fig. 4b shows that near the marking threshold where eraseability is best, the marks are undetectable in secondary electron images. No deviation in compositional uniformity is associated with the amorphization in EDX maps (not shown). Low-temperature cathodoluminescence images of the laser marks confirm that non-radiative recombination is increased in the amorphous regions. Kikuchi patterns from EBSD examination (not shown) indicate crystallinity outside the laser marks but not within, consistent with local amorphization at EBIC minima. The damage seen in secondary images at powers slightly above the amorphization threshold is mainly in the cap layer.

3.3 Erasure and recrystallization of amorphous bits

The simplest way to recrystallize amorphous marks is through furnace annealing of the entire device. In Fig. 5 EBIC results are presented on a row of laser melt-quenched bits before and after furnace-annealing. The annealing furnace was held at 300 °C for 5 mins. Before thermal treatment the marks have an EBIC gain that is about half that of the background, while afterward they are indistinguishable from the matrix signal. The EBIC gain is not zero at the amorphous bits because a 2 keV beam generates a significant number of electron-hole pairs in the remaining crystalline InSe directly below them. Note that at the planned operation energy of 700 eV, most of the electron-hole pairs are generated within the depth of the amorphous bit. The EBIC signal of a defect (scan position $\approx 11.5\ \mu$m in Fig. 5) that is intercepted by the line scan doesn't change significantly, nor does the background level.

The ability to erase amorphous bits in the furnace raises the question of the long-term stability of the marks. A large array of bits was written with near-threshold pulse parameters and examined by EBIC (image not shown). Subsequent to a two-week, 113 °C anneal, the array was examined by EBIC again and found to be unchanged. Epitaxial

InSe/GaSe therefore satisfies the minimum erasibility and archivability requirements for a phase-change medium. The remaining important criteria for traditional optical recording are fast recrystallization and the ability to retain contrast over many cycles.

Contrast retention over 15 cycles using pulsed erasure is demonstrated in Fig. 6. The EBIC image depicts a portion of an array in which different rows have been exposed to a different number of write-erase cycles as indicated on the left side of the image. The first cycle consists of one 5.6 mW, 30 ns amorphization pulse ("I") followed by one 1.8 mW, 1 ms recrystallization pulse ("E"). Subsequent cycles consist of one 4.7 mW, 30 ns re-amorphization pulse ("W") followed by the same recrystallization pulse. Thus "1.5" indicates a pulse sequence of I-E-W, while "2" indicates I-E-W-E. Rows labeled with a half-integer number show a suppression of EBIC signal and are believed to contain amorphous bits. The rows labeled with integer numbers exhibit an EBIC signal similar to that of their original unperturbed state and are believed to be recrystallized. Near-complete erasure is observed out to 15 cycles for probing beam energies from 0.7 to 2 keV, presumably indicating recrystallization throughout the depth of the bit.

That reamorphization requires less power than initial amorphization is perhaps due to reduced thermal conductivity in the re-crystallized state. Use of a lower power for reamorphization reduces damage. While the details of amorphization and erasure differ from sample to sample, the ratio of the best I power to the best E power is always close to 3.

Fig. 7 shows the EBIC gain values out to 15 full cycles that were derived from the array of Fig. 6. These gain values were determined at the center of each mark and averaged at each cycle number. Marks that fell on obvious defects were excluded from the analysis. Note that a contrast of at least 1 gain unit between amorphous and recrystallized states is maintained out to 15 cycles. In Fig. 7 a significant EBIC signal is observed from the amorphous bits because the 2 keV read beam is energetic enough to penetrate below the marks and generate carriers in the underlying crystalline material. A secondary electron image of the array shows no detectable damage, consistent with Fig. 4(b).

Fig. 8 illustrates reversibility of reflectivity and photocurrent through 100 write-erase cycles. The 99.5-cycle marks show more photocurrent contrast with the matrix than those

made with a single amorphization pulse. The behavior in this optical linescan is consistent with 1 keV EBIC images (not shown), where the 99.5-cycle marks appear slightly larger in diameter than the 0.5-cycle marks. The 100-cycle marks appear mostly erased in EBIC at an electron beam energy of 2 keV. However when imaged with a beam energy of 1 keV, the 100-cycle marks look virtually the same as the 99.5-cycle bits. Taken together the various images indicate that while the bulk of the laser-affected region can be amorphized and recrystallized many times, the electronic properties of the surface of the bit may not recover fully after 100 cycles. The incomplete erasure of the surface may be due to damage caused by heating in air. Future use of an inert ambient or vacuum, as well as improved capping layers, may greatly improve erasibility. As discussed in reference to Fig. 6, the use of lower amorphization powers after the first cycle ("W" power $<$ "I" power) can help to prevent damage from repeated cycling and mitigate undesirable growth in the size of the bit. A "W" power $<$ "I" power was not used for Fig. 8. Erasure in the 100th cycle was better for lower amorphization powers.

None of the data described so far bears on the mode of recrystallization of the bits. Both nucleationless regrowth from the crystalline matrix and homogeneous nucleation throughout the amorphous region have been observed in commonly used recording media.[39] The data of Fig. 9 suggest that recovery of the EBIC signal proceeds inward from the edge of the bit. Erase pulses longer than 100 μs produce no further change in the EBIC gain of the mark. These observations are consistent with radial recrystallization of the bit from the crystalline matrix, although EBIC is at best an indirect measurement of crystallinity. The reason that the final EBIC of the erased marks is higher than the original matrix level is obscure although it may be due to a reduction in contact resistance. A final higher EBIC is only observed with pulse annealing (not furnace annealing) and is more reproducible with the 400 nm laser, although bright rings around bits amorphized by the 488 nm laser can be observed in Fig. 6. Recording experiments like those of Fig. 7 but performed with the 400 nm laser show that the enhanced-EBIC recrystallized state persists over many cycles.[40]

Additional evidence for radial regrowth of amorphous bits is provided by *in situ* recrystallization studies in a TEM. The results of such a study are displayed in Fig. 10.

Panel (a) shows the edge of a large mark nominally identical to that illustrated in Fig. 3. In Fig. 10(b), 10 s of irradiation with a 1 μm diameter, 1 MW/cm^2 electron beam has induced radial regrowth from the edge of the crystalline matrix extending about 60 nm towards the bit center. The crystal growth appears quite two-dimensional in keeping with the layered structure of InSe. The recrystallized material consists of several small crystallites separated by stacking faults. In panel (c), which shows the same region after a further 10 s of irradiation, these crystallites are no longer visible. The mode of the recrystallization that occurs between (b) and (c) is not clear; the projection of several crystallites on top of one another in the cross-section may be obscuring this information. These TEM images show that nucleationless recrystallization can occur in the amorphous marks under some circumstances, although the electron-beam heating conditions are not the same as those in either the furnace or laser-pulse erasure experiments. A recent study has shown that in the absence of heating, electron-beam irradiation of GeSbTe optical recording media strongly promotes nucleation without much effect on grain growth.[41)]

Another question is whether the amorphous marks are undergoing solid-state recrystallization or whether they are remelting during the erasure pulse and crystallizing during its trailing edge. Both methods are applicable in tellurium-based phase-change media.[42)] To address this issue, an array of identical amorphous marks on an InSe 100 nm/GaSe 10 nm film with a 3 nm Mo plus 3 nm SiO_2 cap was exposed to erase pulses of the same width (1 ms) and optimized power (1.8 mW) but with trailing edges varying from 100 μs to 12 ns. The photocurrent and reflectivity data (not shown) indicate that marks corresponding to all the trailing edges were equally erased. The absence of any trend in erasure behavior over nearly four orders of magnitude in trailing edge duration proves that the marks cannot be remelting during the erase pulses. If they were remelting, the completeness of recrystallization would depend on the length of time during cooling that the temperature resided in a favorable range for nucleation and/or growth. Because the photocurrent signal recovery depends only on the pulsewidth at peak power, solid-state recrystallization must occur during this constant-power segment of the pulse.

4. Discussion

4.1 Electronic properties of epitaxial diodes

The anisotropic nature of epitaxial InSe and GaSe makes interpretation of recording experiments more complex than comparable experiments on isotropic polycrystalline GeSbTe and InAgSbTe optical storage media. The substantial EBIC and photocurrent signals produced by the InSe/GaSe epitaxial diodes are initially surprising given the need for carrier transport in the low-conductivity direction of the layered materials. Segura *et al.*[36] found that n-type InSe single crystals have a minority diffusion length 33-50 times shorter in the direction perpendicular to the layers. However, epitaxial films are undoubtedly less anisotropic than the bulk single crystals due to a higher density of in-plane defects.[30] A diffusion length of up to 0.2 μm parallel to the c-axis was reported in thin epitaxial InSe films,[25] which is still larger than the thickness of the epilayers in the present study. The layered structure also makes the thermal conductivity anisotropic. One measurement on GaSe single crystals yields a thermal conductivity anisotropy ratio of 10.[43] The higher in-plane than out-of-plane thermal conductivity may increase the diameter of laser marks in thick films somewhat, although the quasi-hemispherical shape of the bit shown in Fig. 3 indicates that this effect is not large.

A diode with 100% efficient charge collection that was measured under the optical illumination conditions of Fig. 1 would exhibit a photocurrent of 27 mA/cm^2. The actual photocurrent at zero bias is 8.3 mA/cm^2 leading to a collection efficiency estimate of 31%. Photoresponse measurements have been previously reported on single-crystal InSe homojunction diodes[36] and heterojunction diodes made by depositing InSe on GaSe single crystals.[25] These authors concentrated on a photovoltaic power-generation application and did not report detailed reverse-bias transport measurements, making a direct comparison difficult.

Assuming a pair-creation energy of 3.9 eV, the measured EBIC gain of 65 at 2 keV shown in Fig. 5 indicates a collection efficiency of over 20% within the crystalline InSe layer.[14] EBIC gains were as high as 15 even at 700 eV, the planned operating energy of the data storage device.[14] Monte Carlo simulations indicate that approximately 58% of

the energy of a 2 keV electron beam is converted to electron-hole pairs in the InSe layer of the diode of Fig. 5.[44] The rest of the energy is dissipated in the form of backscattered electrons or is absorbed in the Mo cap. The simulation indicates that only a minute amount of generation occurs in the underlying Si or GaSe. The photocurrent contains a larger contribution from collection in the Si substrate than the 2 keV EBIC data do, hence the higher charge-collection-efficiency estimate obtained from Fig. 1.

With a reported perpendicular diffusion length of less than 0.2 μm,[25] the factor of ten lower EBIC gain in the diode of Fig. 7 is not surprising given this device's larger thickness (InSe 100 nm/GaSe 10 nm) compared to the device of Fig. 5 (InSe 50 nm/GaSe 5 nm). A detailed picture of the dependence of EBIC gain and contrast on layer thicknesses will require both an improved understanding of carrier transport in the InSe layer and a better device model for the InSe/GaSe heterojunction. The film transport parameters necessary to perform these calculations have not yet been measured.

The data of Fig. 5 demonstrate a contrast of about 25 gain units between amorphous bits and the unpatterned matrix, while that of Fig. 7 for the thicker diode with thicker cap give a contrast modulation of only one gain unit. The contrast in Fig. 5 would be even higher were the electron beam not depositing much of its energy in crystalline material directly below the bottom of the amorphous bit. While the level of contrast in Fig. 7 is not adequate for a working memory device, the larger value in Fig. 5 shows that there is much room for improvement via optimization of the device design and film growth parameters. To date, no such optimization has been performed. In addition, electron beams used for marking should melt smaller amorphous regions which should permit thinner protective caps. Lower losses in thinner, lower atomic number cap layers should increase both EBIC gain and contrast.

4.2 Role of cap layers in marking and read-back

Due to the high sheet resistivity of InSe,[36] the diodes benefit from the presence of conducting cap layers. Mo cap layers on the epitaxial InSe/GaSe/Si devices provide chemical protection and structural stability in addition to improving diode performance. Cycling studies on completely uncapped samples have not been successful either with

GeSbTe optical recording media[45] or with the present InSe/GaSe/Si films. In the GeSbTe case, a 200 nm Al layer added to the media stack gives a significant improvement in reversibility due to better mechanical strength.[45]

If stiffness is what makes Mo a useful cap material, then suppression of surface expansion (or contraction) by the cap may make amorphization-related topographic changes smaller than random fluctuations in the surface profile due to defects and substrate features. This suppression may then explain the lack of consistent topographic changes in the AFM data discussed in § 3.2. The anisotropic elastic and thermal properties of the layered InSe should result in a response to amorphization that is qualitatively different from that of isotropic phase-change media. Since the lattice constant of crystalline InSe is much larger in the surface-normal (00ℓ) direction, amorphous InSe could in fact be denser in the normal direction than in its crystalline state. The elastic response of the anisotropic matrix to the presence of an isotropic amorphous mark may induce recrystallization and limit the long-term stability of ultrasmall bits.

The single-crystal InSe/GaSe diodes had a cap of nearly optically transparent indium oxide.[25] There is no equivalent transparent cap for electron-beam recording. While the optical penetration depth of semiconductors depends strongly on the electronic band structure, the electron-beam penetration depth depends primarily on the mass density[16] and falls rapidly at lower electron-beam energies. The electron penetration depth at sub-keV beam energies is less than 10 nm so that any protective layers must be very thin, unlike the thick transparent cladding layers used in compact disc (CD) and DVD products.[20] Low mass-density capping layers like graphitic carbon are obviously preferable. Laser marking tests in air showed that damage to carbon caps occurred at powers well below the marking threshold of the InSe films even when the carbon was protected by a 5 nm SiO_2 overcoat. Thin SiO_2 layers added to Mo caps did improve erasibility, presumably by reducing oxidation. Graphitic cap layers should be revisited when high-power, focused electron-beam sources in a vacuum environment are available for the writing experiments.

4.3 Optimization of read-back and writing parameters

The observation of reversible contrast in both EBIC and photocurrent measurements demonstrates the ability to modulate the electronic properties of bits with minimal damage to the phase-change medium. Considerable scope for tailoring the device design to optimize contrast exists by varying film thickness and doping, cap layer thickness and composition, device operating bias, and electron-beam read energy. A non-monotonic dependence of EBIC contrast on electron-beam read energy is observed. At very low beam energies, surface recombination due to shallow absorption can reduce the crystalline collection efficiency, while at high energies, most electron-hole pairs are generated below the bottom of the amorphous region. EBIC contrast between the two states is therefore largest at intermediate e-beam energies where most of the electron-hole pairs are generated near the center of the amorphous or recrystallized bit. The 488 nm photocurrent measurements suffer from reduced contrast compared to the EBIC measurements due to the longer penetration depth and consequent larger absorption in the Si substrate, especially for thinner media films.

Erasure with the laser was accomplished only for marks made with amorphization pulsewidths ≤ 50 ns and for marks with diameters ≤ 200 nm. Longer amorphization pulses that produce larger diameter marks may themselves be damaging the media. Alternatively the failure to erase larger diameter marks may be due to the necessity of overheating the center in order to get the boundary to the proper temperature range for nucleation and/or growth. A previous study of GeSbTe optical recording media found that longer amorphization pulses resulted in poorer cycling.[45)] In optical recording studies powers on the order of 1.25 times[21)] and 1.75 times[45)] the melting threshold have been used to enhance the contrast between the two states by increasing the amorphous mark diameter. Fig. 11 shows that flexibility in choosing the write power is small for the thinly capped InSe/GaSe media. Without going to undesirably thick cap layers, the write power can be varied up to at most 1.3 times the melting threshold. The range of allowable erase powers is also tightly constrained. Designing the electron-beam medium device so that the cap layer limits damage during cycling but allows sufficient electron-beam penetration remains a challenge. The margins for the write and erase processes may be larger for the

much smaller diameter marks that will be produced with electron-beam writing.

The optimal reamorphization ("W") power is only 70-80% of the initial melting power (termed "I"). Decreasing the amorphization power after the first cycle compensates for some unknown change in materials properties, preventing surface bit diameter growth, as discussed in reference to Fig. 8, and allowing stable cycling, as demonstrated in Fig. 7. One property that is likely to be permanently changed after the first amorphization-recrystallization cycle is the thermal conductivity, but there are other possibilities. Rubin observed a progressive *decrease* in amorphous bit size with increased cycle number in GeSnTe media.[47] This decrease was ascribed to phase separation at the edge of the molten bit. Surprisingly a higher amorphization power suppressed this phase segregation by lowering viscosity and promoting better intermixing.[47] The phase separation occurred despite the fact that the Ge-Te and Sn-Te liquids are fully miscible. Any number of complex phenomena could occur in the melting and recrystallization of InSe. The peritectic decomposition of InSe, if it occurs rapidly enough, can complicate the melting; or previously identified immiscible In-Se liquids could possibly form.[48] The analysis of erasure mechanisms and failure modes in the epitaxial InSe/GaSe/Si diodes is just beginning and will require a major TEM analysis effort. These studies may also explicate the mechanism of the post-erasure enhancement in EBIC that is observed in some cases, such as Fig. 9c.

4.4 Mode of recrystallization

Attempts to laser-recrystallize amorphous bits formed in films less than 100 nm thick are not yet successful. For these thin films, non-damaging recrystallization pulses shrink the diameter of the mark as in the 10 μs data of Fig. 9b but never completely eliminate EBIC contrast. Longer or higher power pulses cause cap damage. Damage in films that are thin compared to the optical penetration depth may be related to overheating of the GaSe layer or the InSe/GaSe interface. Interdiffusion of InSe and GaSe during film deposition has been observed in previous work[31] and in our films.[30] Problems caused by a long optical penetration depth should be ameliorated when low-energy-electron amorphization becomes possible. An alternative explanation for the failure to erase bits written on thinner films is that the mode of recrystallization may be different. Zhou found that the

erasure time can be strongly dependent on thickness for media less than 50 nm thick.[21] Yet another possibility is a slight difference in the composition of thinner films. InSe layers of 50 nm or less exhibited notably fewer In inclusions than thicker films, as was also noted by previous authors.[25]

Coombs *et al.*[15] and Zhou[21] have used measurements of erasure time as a function of mark diameter to establish whether a given medium is nucleation-dominated or growth-dominated. For nucleation-dominated media, the complete erasure time is nearly independent of mark diameter, while for growth-dominated media, the erasure time decreases exponentially with decreasing diameter.[49,50] Unfortunately this decisive experiment for determining the mode of recrystallization is inapplicable to InSe/GaSe due to the limited diameter range of erasable amorphous marks, as discussed in regard to Fig. 11. (A laser-marking system with shorter pulses or controlled defocus could potentially make smaller amorphous marks, but these capabilities are not available.) The images of Fig. 10 are strongly suggestive of growth-dominated behavior but are not conclusive. Growth-dominated behavior that produces a nearly single-crystalline erased bit would not be a surprise given the complete recovery of the EBIC and photocurrent signals. According to the classical theory of crystallization, the probability of nucleation will peak just above the glass transition temperature since the driving force for the formation of the crystalline phase is highest at the lowest temperatures.[49,50] At higher temperatures the size of the smallest stable nucleus is larger and nucleation becomes less probable. Growth on the other hand can be peaked at any temperature between the glass transition temperature and the melting temperature. Thus the low-temperature furnace anneal of Fig. 5 may proceed by nucleation-and-growth while the higher-temperature pulsed erasure may proceed by growth from the edge of the bit. The temperature of the furnace anneal (300 °C) is close to the temperature used for crystallization of as-deposited amorphous films via nucleation-and-growth.[19]

The 2 μs complete optical erasure time reported by Nishida *et al.* for polycrystalline In-Se films[51] is quite short compared to the minimum 100 μs observed for InSe/GaSe/Si to date. Nishida *et al.* used an 830 nm laser with a final objective of NA = 0.5,[19] so clearly their marks were much larger in diameter than those of the present study, while

their films were 120 nm in thickness,[19] similar to our InSe/GaSe/Si. Nishida and co-workers found that the erasure time is only weakly dependent on composition and that it increases with increasing write power,[19] both of which are signs of growth-dominated recrystallization.[52] X-ray diffraction data in both these earlier studies indicate that the alloy films were non-stoichiometric and polyphase, so it is possible that an unknown fast recrystallizing or unamorphized impurity phase plays a role. However, the broad composition range over which short erasure times are observed in the polycrystalline films makes this explanation seem less likely. A more probable answer is that the polycrystalline In-Se films are heterogeneously nucleating on the ZrO_2 or SiO_2 dielectric layers with which they were clad.[19,51,53] Ohshima has demonstrated that dielectric layers can significantly accelerate nucleation at interfaces.[54]

The growth-dominated InAgSbTe optical recording media are close to the eutectic composition in the Sb-Te phase diagram.[49,50] A minimum erasure time has also been observed near the $In_{46}Te_{54}$ eutectic.[55] At a eutectic point, nucleation of the solid phase is least favorable because the liquid achieves its maximum stability. The In-Se phase diagram has no eutectic point so it's reasonable to wonder whether growth-dominated behavior is likely in this alloy system. However Coombs *et al.* have shown that the only requirement for growth-dominated behavior is suppression of nucleation, and that this suppression can be achieved by a wide variety of dopants in the GeSbTe system, for example by adding Ge, S or Se at the few percent level.[52] Growth-dominated recrystallization is therefore a fairly general phenomenon whether nucleation is suppressed thermally or by impurities.

The mode of recrystallization is a crucial question for the future application of the InSe/GaSe phase-change medium. The observed minimum recrystallization time of 100 μs would pose an unacceptable data rate limitation on any future storage device. If the recrystallization mode is growth-dominated, then an exponential speed-up in complete erasure time is anticipated at the much smaller bit diameters that will be possible with electron-beam writing. If the recrystallization mode is nucleation-dominated, then smaller bit diameters may not improve the erasure time sufficiently. Clearly this is an area for intensive future study.

5. Conclusions

We have demonstrated a read-back mechanism that enables electron-beam data storage on phase-change media. A silicon-processing-compatible medium device based on an epitaxial InSe/GaSe heterojunction diode has been constructed and a current gain of 65 has been demonstrated at 2 keV beam energy. Bits as small as 100 nm in diameter have been observed with a contrast of up to 25 gain units although serious noise problems occur in some films due to the presence of In precipitates. These small bits can sustain 15 write-erase cycles without loss of contrast, and up to 100 cycles have been demonstrated with some contrast degradation. The fastest observed complete erasure time for the amorphous bits is 100 μs, although much shorter erasure times may be possible with smaller diameter bits if the recrystallization is growth-dominated. Major remaining challenges include controlling media defects, reducing the erasure time and designing a cap layer that will minimize damage during cycling without severely attenuating the low-energy electron read-back beam. Upcoming electron-beam marking experiments should provide more information on the minimum stable amorphous bit size, the smallest bit depth for which usable EBIC contrast is observed, and the diameter dependence of the recrystallization time. These measurements will indicate the maximum practical storage density for electron-beam recording on phase-change media. The InSe/GaSe/Si medium should also be considered for use in ultra-high density optical memories[4,5,9] with an optical write, electrical read-back scheme.

Acknowledgements

We would like to thank R. Bicknell-Tassius for film deposition and many useful discussions and H. Birecki for design and construction of the 488 nm laser marking system. Dr. J. F. Sánchez-Royo of the Universitat de València helped us immeasurably by providing InSe/GaSe single-crystal samples. We acknowledge T. N. Hurst for informative discussions about optical recording, P. E. A. Turchi of LLNL for helpful advice about phase diagram interpretation and R. Gauvin of McGill University for assistance with Monte Carlo calculations. We would like to thank H. Liao for device fabrication and A. P. Holden for bandwidth measurements. M. D. Flores deposited the top contacts, P. Bacon

performed some of the X-ray diffraction experiments and M. Setera did some of the EBIC measurements. J. Washburn and W. Swider of LBNL assisted in preparation of TEM specimens. The authors would like to thank the National Center for Electron Microscopy at LBNL for the opportunity to use its facilities.

References

1) G. A. Bertero, S. Malhotra, B. Bian, J. Tsoi, M. Avenell, D. Wachenschwanz and T. Yamashita: IEEE Trans. Magn. **39** (2003) 651.
2) T. Iwanaga, S. Ohkubo, M. Nakano, M. Kubota, H. Honma, T. Ide and R. Katayama: Jpn. J. Appl. Phys. **42** (2003) 1042.
3) E. Betzig, J.K. Trautman, R. Wolfe, E. M. Gyorgy, P. L. Finn, M. H. Kryder and C.-H. Chang: Appl. Phys. Lett. **61** (1992) 142.
4) I. D. Nikolov: Nanotechnology **15** (2004) 1076.
5) B. D. Terris, H. J. Mamin, D. Rugar, W. R. Studenmund and G. S. Kino: Appl. Phys. Lett. **65** (1994) 388.
6) S. Hosaka, T. Shintani, M. Miyamoto, A. Kikukawa, A. Hirotsune, M. Terao, M. Yoshida, K. Fujita and S. Kämmer: J. Appl. Phys. **79** (1996) 8082.
7) D. Saluel, J. Daval, B. Bechevet, C. Germain and B. Valon: J. Magn. Magn. Mater. **193** (1999) 488.
8) O. Bichet, C. D. Wright, Y. Samson and S. Gidon: J. Appl. Phys. **95** (2004) 2360.
9) Afshin Partovi, David Peale, Matthias Wuttig, Cherry A. Murray, George Zydzik, Leslie Hopkins, Kirk Baldwin, William S. Hobson, James Wynn, John Lopata, Lisa Dhar, Rob Chichester, and James H-J Yeh: Appl. Phys. Lett. **75** (1999) 1515.
10) R. Bennewitz, J. N. Crain, A. Kirakosian, J.-L. Lin, J. L. McChesney, D. Y. Petrovykh and F. J. Himpsel: Nanotechnology **13** (2002) 499.
11) P. Vettiger and G. Binnig: Sci. Am. **288** (2003) 46.
12) S.-T. Lam: J. Vac. Sci. Techn. **B21** (2003) 479.
13) S.-T. Lam: US Patent #5,557,596.
14) G. A. Gibson, A. Chaiken, K. Nauka, C. C. Yang, R. Bicknell, B. S Yeh, J. Chen, H. Liao, J. Jasinski, Z. Liliental-Weber, R. Davidson, A. Holden, S. Subramanian and D. Schut: Appl. Phys. Lett. **86** (2005) 051902.
15) J. H. Coombs, A. P. J. M. Jongenelis, W. van Es-Spiekman and B. A. J. Jacobs: J. Appl. Phys. **78** (1995) 4906.
16) E. Grunbaum, E. Napchan, Z. Barkay, K. Barnham, J. Nelson, C. T. Foxon, J. S.

Roberts and D. B. Holt: Semicond. Sci. Technol. **10** (1995) 627.

17) J. Rechid, A. Kampmann and R. Reineke-Koch: Thin Solid Films **361** (2000) 198.
18) M. Chen, K. A. Rubin and R. W. Barton: Appl. Phys. Lett. **49** (1986) 502.
19) T. Nishida, M. Terao, Y. Miyauchi, S. Horigome, T. Kaku and N. Ohta: Appl. Phys. Lett. **50** (1987) 667.
20) M. Horie, N. Nobukuni, K. Kiyono and T. Ohno: Proc. SPIE **4090** (2000) 135.
21) G.-F. Zhou: Mater. Sci. Eng. **A304-306** (2001) 73.
22) G. A. Gibson, H. Birecki, S. L. Naberhuis and A. Chaiken: unpublished.
23) H. N. Bertram and Q. Peng: IEEE Trans. Magn. **34** (1998) 1543.
24) S. El Monkad, M. Eddrief, J. P. Lacharme, K. Amimer and C. A. Sebenne: Surf. Sci. **352-354** (1996) 833.
25) J. F. Sánchez-Royo, A. Segura, O. Lang, E. Schaar, C. Pettenkofer, W. Jaegermann, L. Roa and A. Chevy: J. Appl. Phys. **90** (2001) 2818.
26) J. E. Palmer, T. Saitoh, T. Yodo and M. Tamura: J. Cryst. Growth **147** (1995) 283.
27) W. Jaegermann, A. Klein and C. Pettenkofer: *Electron Spectroscopies Applied to Low-Dimensional Materials*, ed. H.P. Hughes and H.I. Starnberg (Kluwer Academic, Dordrecht, 2000).
28) N. Nakayama, T. Kuramachi, T. Tanbo, H. Ueba, and C. Tatsuyama: Surf. Sci. **244** (1991) 58.
29) L. Brahim Otsmane, J. Y. Emery, M. Jouanne and M. Balkanski: Appl. Surf. Sci. **65/66** (1993) 479.
30) J. Jasinski, Z. Liliental-Weber, A. Chaiken, G. A. Gibson, K. Nauka, C. C. Yang and R. Bicknell-Tassius: Mater. Res. Soc. Proc. Symp. **803**, ed. J. Ahner, L. Hesselink and J. Levy (2003).
31) M. Budiman, A. Yamada and M. Konagai: Jpn. J. Appl. Phys. **37** (1998) 4092.
32) J. Ager, J. Wu, K.M. Yu, W. Walukiewicz and K. Nauka: unpublished results.
33) C. Ulrich, D. Olguin, A. Cantarero, A. R. Goni, K. Syassen and A. Chevy: Phys. Status Solidi **B 211** (2000) 777.
34) F. J. Manjón, Y. van de Vijver, A. Segura, V. Muñoz, Z. X. Liu and C. Ulrich: Phys. Status Solidi **B 211** (1999) 104.

35) A. M. Gabor, J. R. Tuttle, D. S. Albin, M. A. Contreras, R. Noufi and A.M. Hermann: Appl. Phys. Lett. **65** (1994) 198.

36) A. Segura, J. P. Guesdon, J. M. Besson and A. Chevy: J. Appl. Phys. **54** (1983) 876.

37) J. F. Sánchez-Royo, A. Segura, A. Chevy and L. Roa: J. Appl. Phys. **79** (1996) 204.

38) V. Weidenhof, I. Friedrich, S. Ziegler and M. Wuttig: J. Appl. Phys. **86** (1999) 5879.

39) Y. Nishi, H. Kando and M. Terao: Jpn. J. Appl. Phys. **41** (2002) 631.

40) S. Subramanian: unpublished.

41) B. J. Kooi, W. M. G. Groot and J. Th. M. De Hosson: J. Appl. Phys. **95** (2004) 924.

42) C. A. Volkert and M. Wuttig: J. Appl. Phys. **86** (1999) 1808.

43) K. Maschke and F. Lévy: *Landolt-Börnstein New Series Group III*, ed. O. Madelung, M. Schulz and H. Weiss (Springer Verlag, Berlin, 1984), Vol. 17f, p. 304.

44) P. Hovington, D. Drouin and R. Gauvin: Scanning **19** (1997) 1.

45) K. A. Rubin, D. P. Birnie III and M. Chen: J. Appl. Phys. **71** (1992) 3680.

46) K. Shimakawa, A. Kolobov and S. R. Elliott: Adv. Phys. **44** (1995) 475.

47) K. A. Rubin: Mater. Res. Soc. Symp. **230** (1992) 239.

48) *Binary Alloy Phase Diagrams*, ed. T. B. Massalski, H. Okamoto, P. R. Subramanian, and L. Kacprzak (ASM International, Materials Park, OH, 1990).

49) G. F. Zhou, H. J. Borg, J. C. N. Rijpers, M. H. R. Lankhorst and J. J. L. Horikx: Proc. SPIE **4090** (2000) 108.

50) G. F. Zhou and B. A. J. Jacobs: Jpn. J. Appl. Phys. **38** (1999) 1625.

51) T. Nishida, M. Terao and M. Nakazawa: Jpn. J. Appl. Phys. **26** (1987) Suppl. 26-4, 67.

52) J. H. Coombs, A. P. J. M. Jongenelis, W. van Es-Spiekman and B. A. J. Jacobs: J. Appl. Phys. **78** (1995) 4918.

53) M. Terao, T. Nishida, Y. Miyauchi, S. Horigome, T. Kaku and N. Ohta: Proc. SPIE **695** ()1986) 105.

54) N. Ohshima: J. Appl. Phys. **79** (1996) 8357.

55) Y. Sugiyama, R. Chiba, S. Fujimori and N. Funakoshi: J. Non-Cryst. Solids **122** (1990) 83.

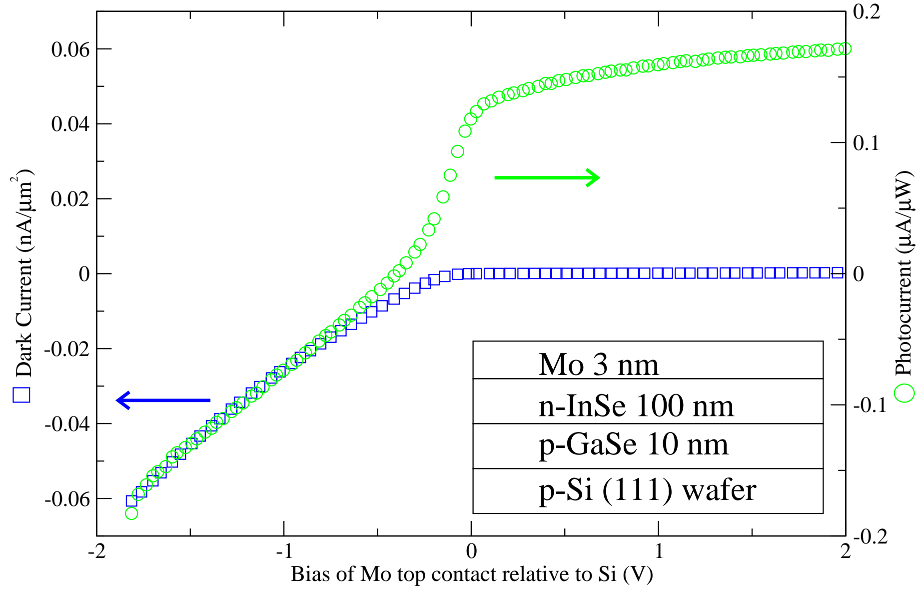

Figure 1: Dark and illuminated I-V curves for an InSe 100 nm/GaSe 10 nm/p-Si(111) heterojunction diode. The Mo top contact is 2 mm in diameter. The illuminated region is a focused 70 μW 488 nm laser spot that is incident on 3×10^{-8} of the total contact area. The inset shows the structure of the device. The dark current is normalized to the contact area while the photocurrent is normalized to the illumination power. The illumination is incident on the device through the thin contact layer.

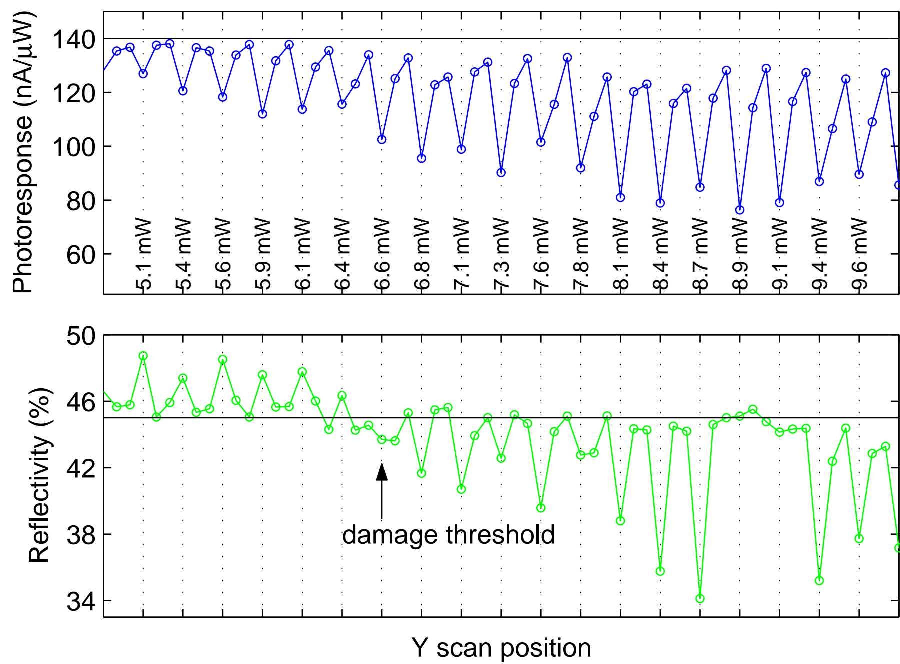

Figure 2: Line scans showing the photocurrent and reflectivity of a row of marks previously generated with a 488 nm laser using square 30 ns pulses of increasing power. The traces were acquired simultaneously while scanning the laser over the marks at a DC power of 70 μW. The marks are recorded in a 100 nm InSe layer deposited on 10 nm of GaSe grown on a Si(111) substrate. The dashed vertical lines show the positions of the laser marks, which are separated by 0.9 μm. The solid horizontal lines show the value of the photocurrent (140 nA/μW) and reflectivity (45%) for the undisturbed matrix. For powers of 6.4 mW or less, the marks correspond to photocurrent minima and reflectivity maxima. For powers of 6.8 mW or more, the marks correspond to reflectivity minima. 6.6 mW is believed to be the damage threshold. There is no recovery of either signal at higher powers that would indicate melt-recrystallization.

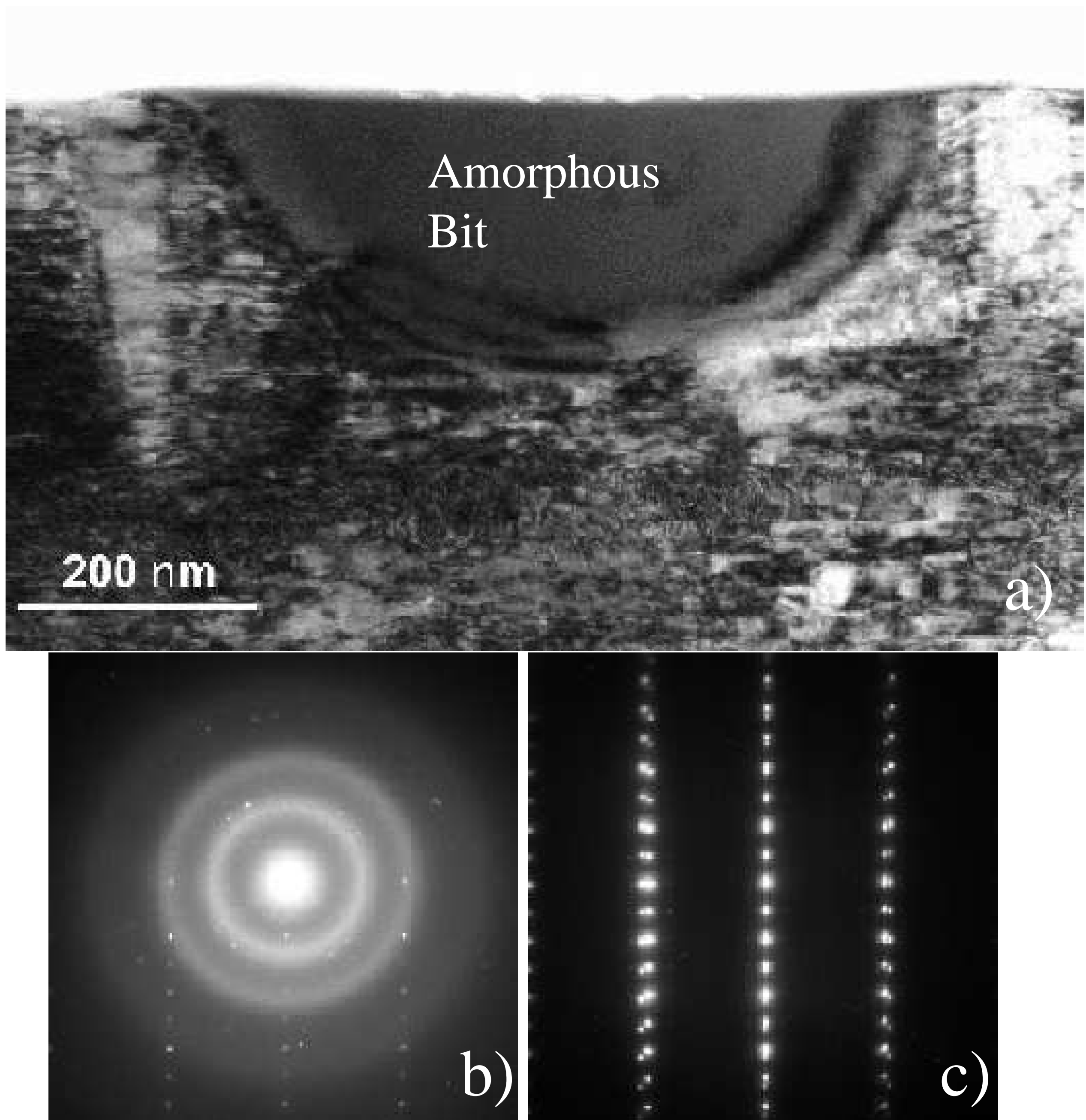

Figure 3: Cross-sectional TEM images of an amorphous laser mark made with a 13.6 mW, 1 μs 488 nm laser pulse on a 350 nm InSe/200 nm GaSe/p-Si(111) device with a 200 nm SiO_2 cap. The cap is not visible in the image. (a) The mark is 630 nm in diameter at the surface and 180 nm deep. The surface of the bit is at the top of the image. (b) Rings in a selected-area diffraction pattern from the mark demonstrate that it is amorphous. Some weak diffraction spots are believed to come from crystalline material in the same transmission column as the amorphous material. (c) A selected-area diffraction pattern from the matrix surrounding the mark has peaks that index well to layered, c-axis-oriented

rhombohedral InSe.[30]

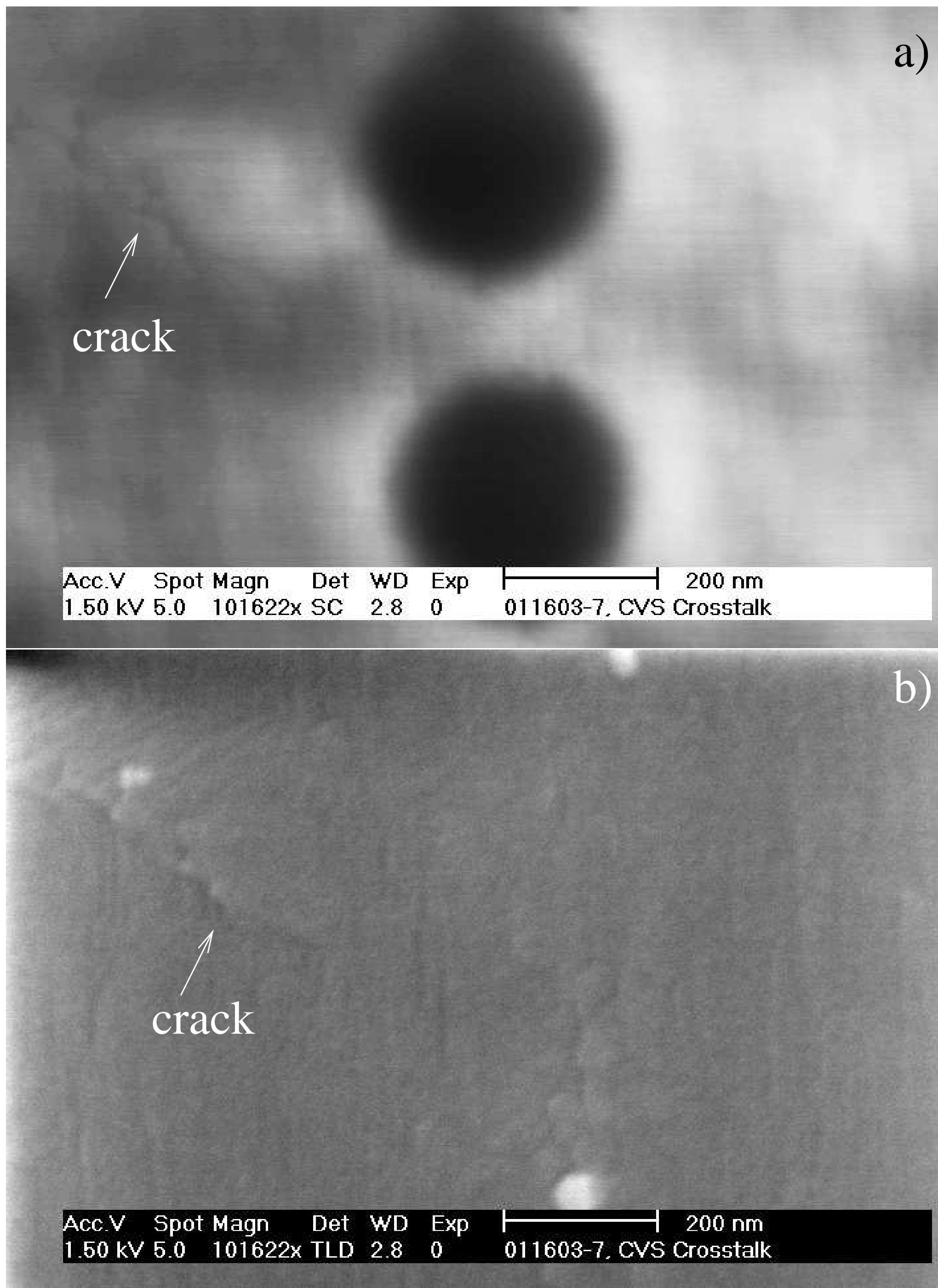

Figure 4: (a) A 1.5 keV EBIC image of two amorphous marks made on an InSe 100 nm/GaSe 10 nm film with an 8 nm Mo + 5 nm SiO_2 cap. (b) A secondary electron image of the same region showing that minimal damage occurs near the laser marking threshold. A small crack is evident in both two images.

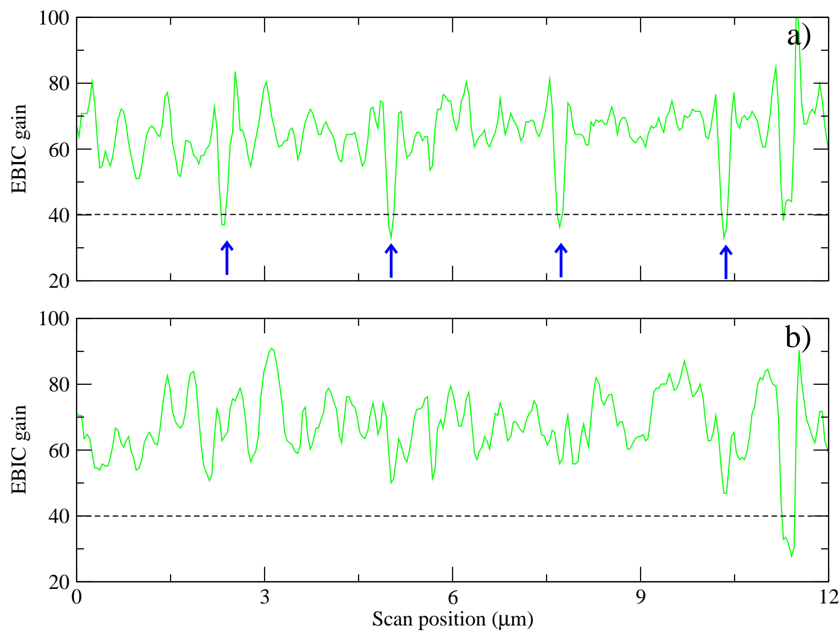

Figure 5: 2 keV EBIC line scans through the same row of nominally identical laser marks (a) before and (b) after furnace annealing. Amorphous marks are indicated by arrows in (a). Before the anneal, all of the laser marks had an EBIC gain less than 40 while afterwards the marks are indistinguishable from the background. The device is an InSe 50nm/GaSe 5 nm film with a tapered Mo cap. Marks of 150 nm diameter were made with 5 mW, 40 ns pulses using the 400 nm laser. The anneal was performed at 300 °C for 5 mins.

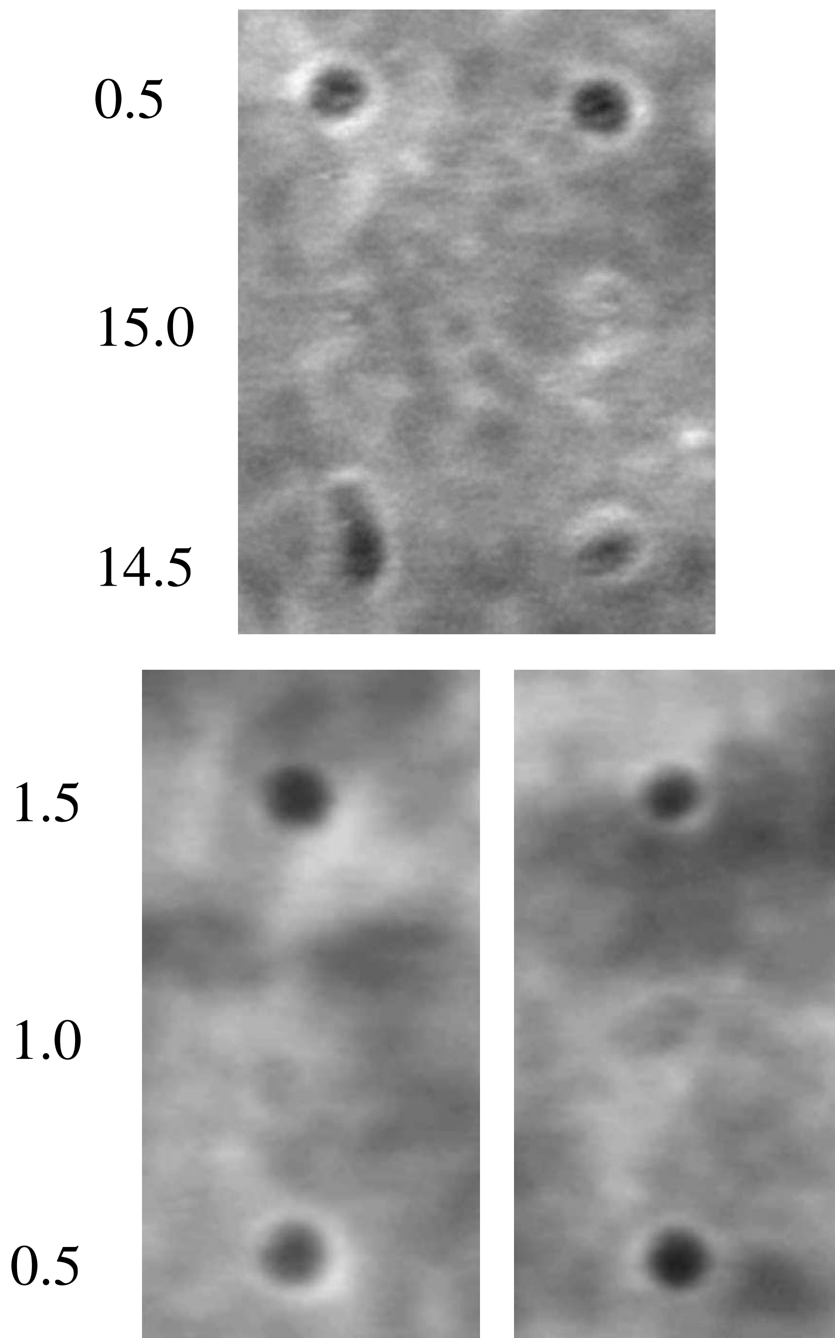

Figure 6: 2 keV EBIC images of an array of laser marks made on an InSe 100 nm/GaSe 10 nm film using 5.6 mW, 30 ns initial amorphization pulses (I), 4.7 mW, 30 ns W reamorphization pulses (W) and 1.8 mW, 1 ms E crystallization pulses (E) with the 488 nm laser. The left column gives the number of write-erase cycles for the row of marks to its right. Fifteen cycles were written at different locations in this array but only a few rows are shown here for clarity. The "0.5," "1.5" and "14.5" rows show a consistently reduced EBIC signal and are presumed to be amorphous. The "1.0" and "15.0" rows are nearly invisible and are presumed to be recrystallized. The center-to-center mark spacing

is 1 μm. The device has a 3 nm Mo plus 3 nm SiO_2 cap.

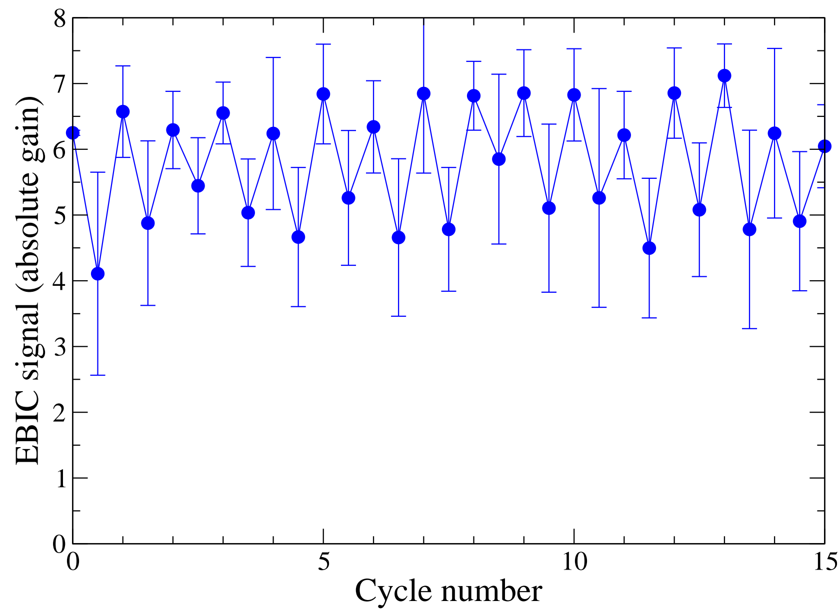

Figure 7: A plot of EBIC gain at 2 keV vs. cycle number for the laser marks shown in Fig. 6. The first pulse was made with the I conditions. Other half-integer cycles end in an amorphization (W) pulse, while integer cycles end in a recrystallization (E) pulse. A modulation of about 1 gain unit is maintained out to 15 cycles. Error bars indicate the variance that is attributable to crystalline defects in the InSe film. The gain at cycle 0 is that of the unperturbed matrix.

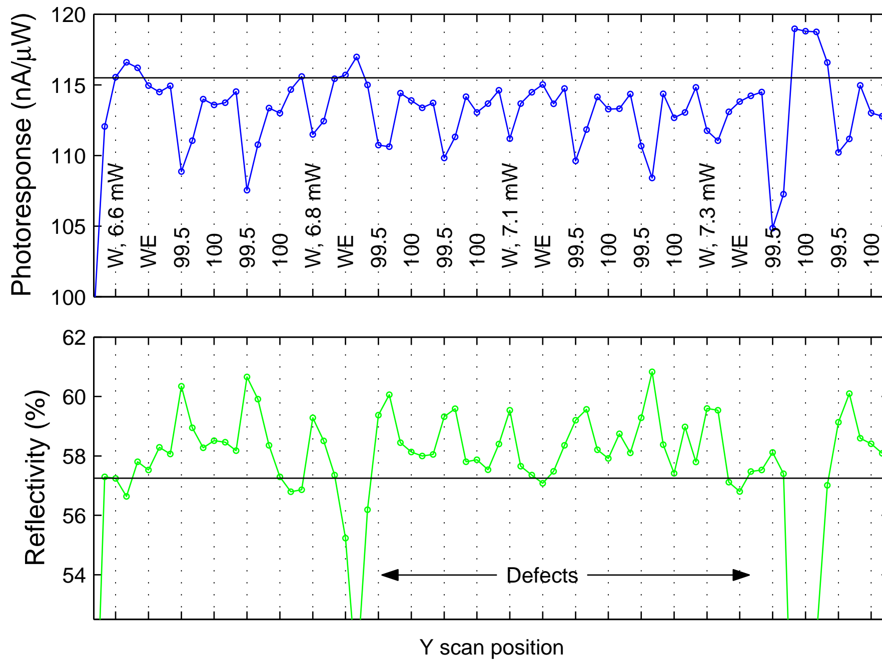

Figure 8: A line scan through a row of 488 nm laser marks (centered at vertical dotted lines) of varying W powers and number of cycles up to 100. For each of the W powers, the 99.5-cycle marks correspond to a photocurrent minimum and a reflectivity maximum while the 100-cycle and WE marks are close to the matrix level in both the reflectivity and photocurrent channels. The 6.6 mW W-only mark overlaps with the edge of a large-diameter fiducial mark and is missing, but all the other nominally amorphous marks are distinct. The device is an InSe 100 nm/GaSe 10 nm film with a 5 nm Mo plus 5 nm SiO_2 cap. The same power was used for the initial amorphization as for subsequent re-amorphizations. The E pulses use 2.2 mW power and 1 ms pulsewidth. The horizontal lines show the photocurrent and reflectivity levels of the unperturbed matrix.

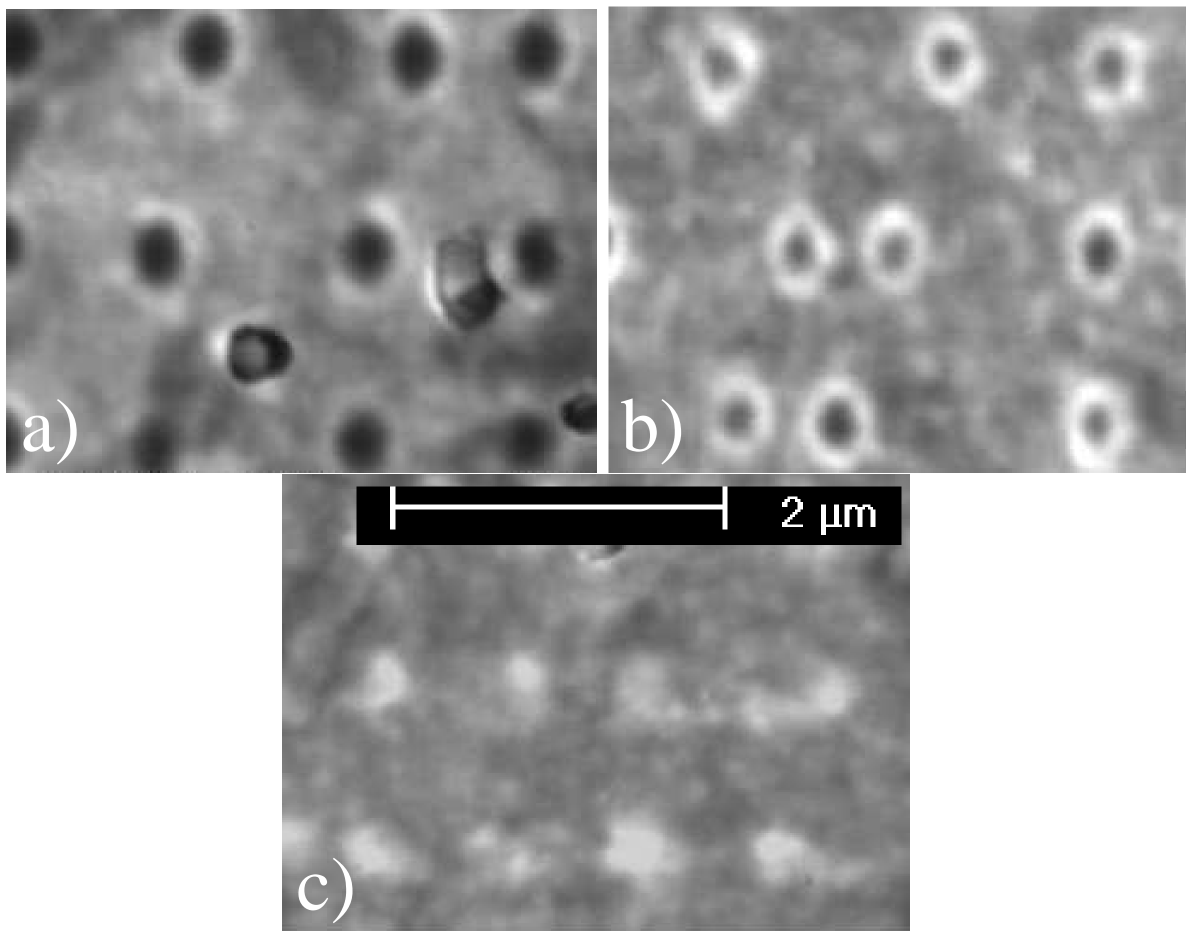

Figure 9: (a) Amorphous bits created with 5 mW, 50 ns amorphization pulses from the 400 nm laser on a film with a tapered Mo cap. The marks are EBIC signal minima surrounded by a thin bright ring of enhanced signal. (b) Marks made with two pulses: the same 50 ns pulse as in (a), plus a second 1 mW, 10 μs erase pulse. The ring of enhanced EBIC has extended inward at the expense of the dark center. (c) The same as (b), but with 100 μs erase pulses. The dark centers are now completely gone and the marks are converted into EBIC maxima. All EBIC images were taken with a 2 keV beam energy. Different areas of the same film are shown in the three images.

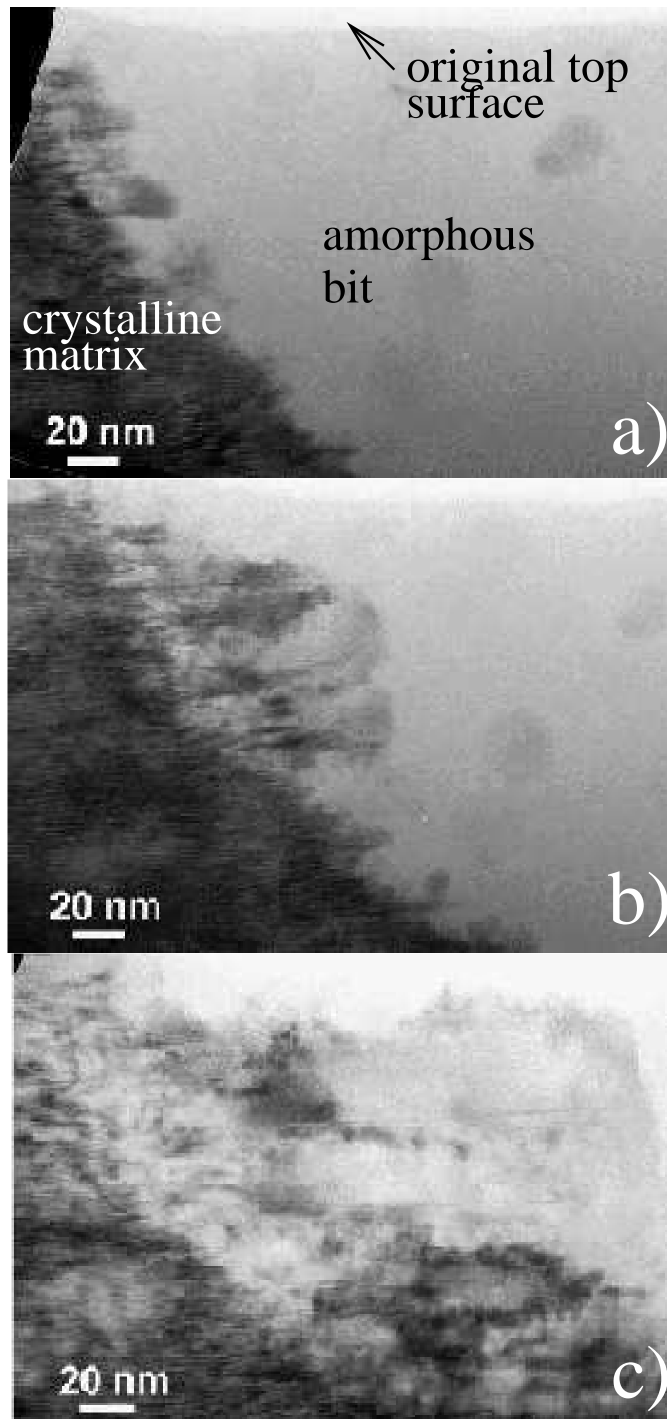

Figure 10: A series of cross-sectional TEM images of the edge of a laser mark similar to that shown in Fig. 3. (a) Unirradiated; high-magnification image of the same state shown in Fig. 3a. The layered morphology of the crystalline matrix is clearly visible. (b) After 10 s of intense irradiation, the small crystallites shown at the left edge of the mark in (a) have advanced about 60 nm toward the center of the mark. The pre-existing crystallites in (a) are unchanged. (c) After a further 10 s of irradiation, the mark is completely recrystallized. Whether some homogeneous nucleation has occurred in addition to the

observed regrowth from the edge is not clear.

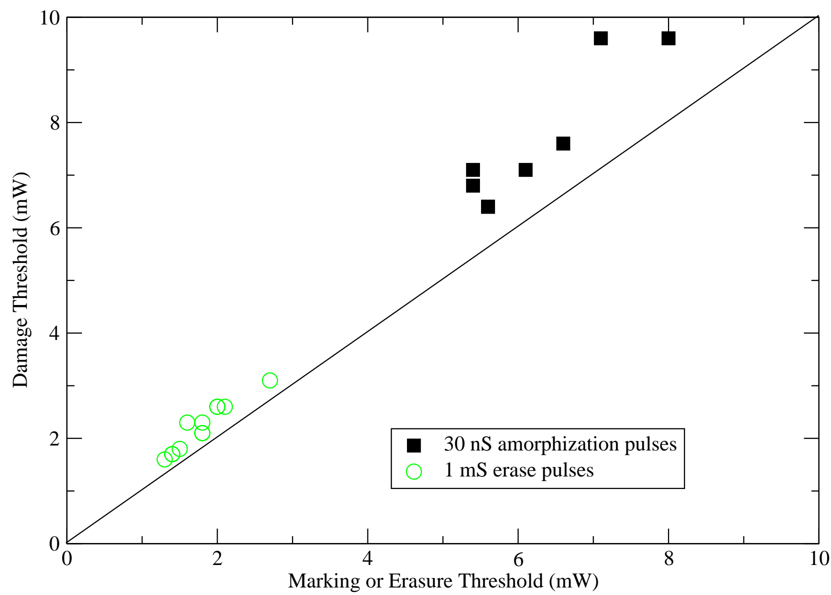

Figure 11: A plot of the damage threshold vs. the marking or erasure threshold for some InSe/GaSe devices using the 488 nm laser. The damage threshold is determined by observation of a large, discontinuous change in the reflectivity and/or photocurrent versus pulse power. The vertical distance between the data points and the diagonal line is the margin for the process. The thicker the cap layer of a device, the wider the range of pulse parameters that it could tolerate without irreparable harm. The largest margin for the 30 ns write pulses corresponds to an 8 nm Mo cap layer which is thick enough to significantly reduce contrast during electron-beam read-back.